Chapter 2
Bayesian Modelling of Offshore Platforms

P.L. Green, U.T. Tygesen, and N. Stevanovic

Abstract This paper details a case study, where Bayesian methods are used to estimate the model parameters of an offshore platform. This first involves running a series of Finite Element simulations using the Ramboll Offshore Structural Analysis Programs (ROSAP)—developed by Ramboll Oil & Gas—thus establishing how the modal characteristics of an offshore structure model vary as a function of its material properties. Data based modelling techniques are then used to emulate the Finite Element model, as well as estimates of model error. The uncertainties associated with estimating the hyperparameters of the data based modelling techniques are then analysed utilising Markov chain Monte Carlo (MCMC) methods. The resulting analysis takes account of the uncertainties which arise from measurement noise, model error, model emulation and parameter estimation.

Keywords System identification • Model updating • Offshore platform • Gaussian process • Uncertainty quantification

2.1 Introduction

Ramboll Oil & Gas utilise bespoke Finite Element (FE) software [1] to estimate the fatigue damage present in offshore platforms. Before such an assessment can take place the parameters of the FE model are updated, using measurement data, in two phases. The first stage involves using measured modal data to update parameters which, for example, represent the stiffness or centre of gravity (COG) of the offshore structure. With the second stage, other key parameters are updated using measurements which relate wave loading to the stresses measured at certain points on the platform.

This paper is the starting point of a longer term project, which aims to quantify and propagate the uncertainties involved in both of these states of model updating. The current work is concerned with the situation where modal data is used to infer the COG of the platform. (This is necessary because, as a result of the accumulation of unregistered equipment and/or expansion projects, the COG is often difficult to measure accurately.) Specifically, it focuses on then scenario where a sparse set of measurements are available and, because of computational constraints, only a limited number of FE simulations are possible. It utilises the fundamental framework which, originally proposed in [2], will now be described within the context of the current problem.

The vector $\boldsymbol{x}_i$ is used to denote the ith measurement of the first ten natural frequencies of an offshore platform while z_i represents a corresponding measurement of the platform's COG (for now, in this preliminary work, only the vertical position of the COG will be considered). A total of n measurements are available. It is assumed that z_i and $\boldsymbol{x}_i$ are related by

$$z_i = y(\boldsymbol{x_i}) + \eta(\boldsymbol{x_i}) + \epsilon, \qquad \epsilon \sim \mathcal{N}(0, \lambda^{-1}), \qquad i = 1, \ldots, n \tag{2.1}$$

P.L. Green (✉)
Institute for Risk and Uncertainty, Centre for Engineering Sustainability, School of Engineering, University of Liverpool, Liverpool L69 3GQ, UK
e-mail: p.l.green@liverpool.ac.uk

U.T. Tygesen
Ramboll Oil & Gas, Willemoesgade 2, Esbjerg 6700, Denmark
e-mail: utt@ramboll.com

N. Stevanovic
Siemens Wind Power, Borupvej 16, Brande 7330, Denmark
e-mail: Nevena.stevanovic@siemens.com

S. Atamturktur et al. (eds.), *Model Validation and Uncertainty Quantification, Volume 3*, Conference Proceedings of the Society for Experimental Mechanics Series, DOI 10.1007/978-3-319-29754-5_2

where $y(\boldsymbol{x_i})$ is the output of the FE model, ϵ is measurement noise and η represents *model error*—the inevitable discrepancy between the response of the FE model and that of the real structure. The approach outlined in [2] uses data based modelling techniques—Gaussian processes (GPs) specifically[1]—to achieve two things. Firstly, they are used to interpolate between measurements of model error, thus providing an estimate of η in regions where measurements are unavailable. Secondly, they are used to emulate the expensive FE model, thus reducing the computational cost of the model updating procedure. The aim of this paper is to investigate whether, by applying the methods described in [2], it is possible to realise parameter estimates which are more accurate than those that can be realised simply by interpolating between available measurements.

The paper is organised as follows. A brief description of the FE simulations used in this paper are given in Sect. 2.2. The full model updating procedure is described in detail in Sect. 2.3 before results are presented and discussed in Sects. 2.4 and 2.5 respectively.

2.2 FE Model

The FE analysis was performed using the in-house Ramboll Oil & Gas software, ROSAP. The vast majority of all offshore jackets, topsides, offshore bridges and risers within the Danish oil and gas sector in the North Sea have been analysed and certified by use of the ROSAP. It is currently used to facilitate a large range of analyses including push-over analysis, ship impact analysis, deterministic/transient/spectral fatigue analysis as well as Risk- and Reliability based Inspection Planning software (RBI).

For the present study, a FE model of a typical offshore platform has been used as a basis for data generation. In this case the FE analysis has been used to compute the variation in the first ten natural frequencies of an offshore platform as a function of the vertical offset of its COG (Fig. 2.1). Typically, through model updating, the FE model would then be used to track how the COG changes with time (as a result of well intervention operations, for example). In the analysis described here it is shown how, through the addition of even a sparse number of measurements, this analysis can be greatly improved.

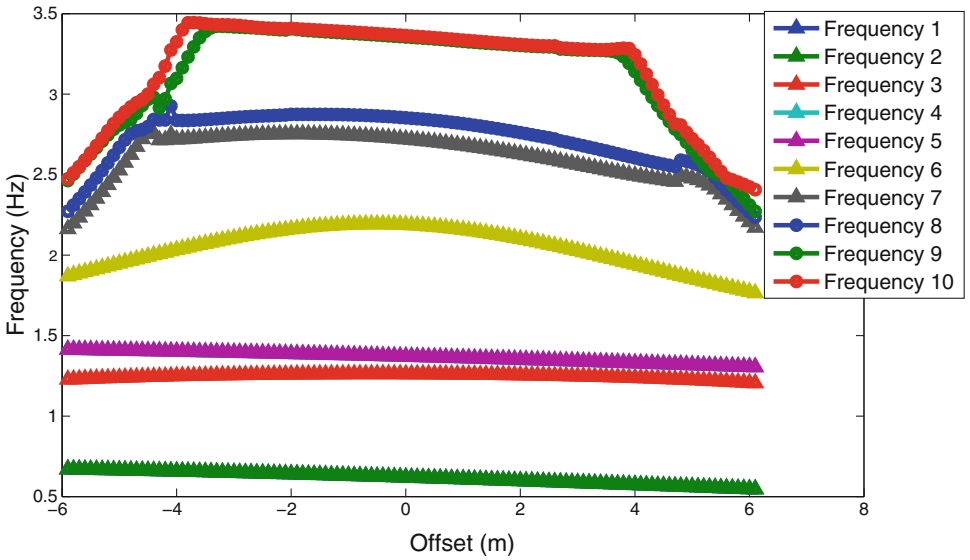

Fig. 2.1 Finite element results

[1] A detailed introduction to Gaussian processes is a little beyond the scope of this paper. For the interested reader, the books [3, 4] are recommended.

2.3 Bayesian Modelling

2.3.1 Available Data

It was found that the FE model predicted a 1–1 relationship between the first natural frequency of the platform and the offset of the COG (shown as blue dots in Fig. 2.2). As a result, for the remainder of this work, it will be assumed that measurements of the first natural frequency only are needed to predict the position of the COG. The frequencies and offset values that were investigated using the FE model are concatenated into the vectors $\boldsymbol{x'} = (x'_1 \quad \dots \quad x'_N)^T$ and $\boldsymbol{y} = (y(x'_1) \quad \dots \quad y(x'_N))^T$ respectively. This relationship between $\boldsymbol{x'}$ and $\boldsymbol{y}$ will be emulated by a GP with prior

$$p(\boldsymbol{y}) = \mathcal{N}(\boldsymbol{0}, \boldsymbol{K_1}) \tag{2.2}$$

where the ijth element of $\boldsymbol{K_1}$ is given by the kernel function

$$k_1(x'_i, x'_j) = \exp\left(-\frac{\alpha_1}{2}(x'_i - x'_j)^2\right) \tag{2.3}$$

where α_1 is a hyperparameter. The n measurements of the first natural frequency and COG offset, denoted $\boldsymbol{x} = (x_1 \quad \dots \quad x_n)^T$ and $\boldsymbol{z} = (z_1 \quad \dots \quad z_n)^T$, are shown as black circles in Fig. 2.2. These observations were created artificially, so that the true relationship between the first natural frequency of the platform and the COG offset could be observed (for validation purposes). The true relationship is shown as a red line in Fig. 2.2. The observations are samples from this true relationship, which have been corrupted with Gaussian noise whose precision, λ, was set equal to 10.

2.3.2 Model Error

With n measurements available, there are therefore n measurements of model error, denoted $\boldsymbol{\eta} = (\eta(x_1) \quad \dots \quad \eta(x_n))^T$. This relationship between input and model error will also be emulated by a GP, with prior:

$$p(\boldsymbol{\eta}) = p(\boldsymbol{0}, \boldsymbol{K_2}) \tag{2.4}$$

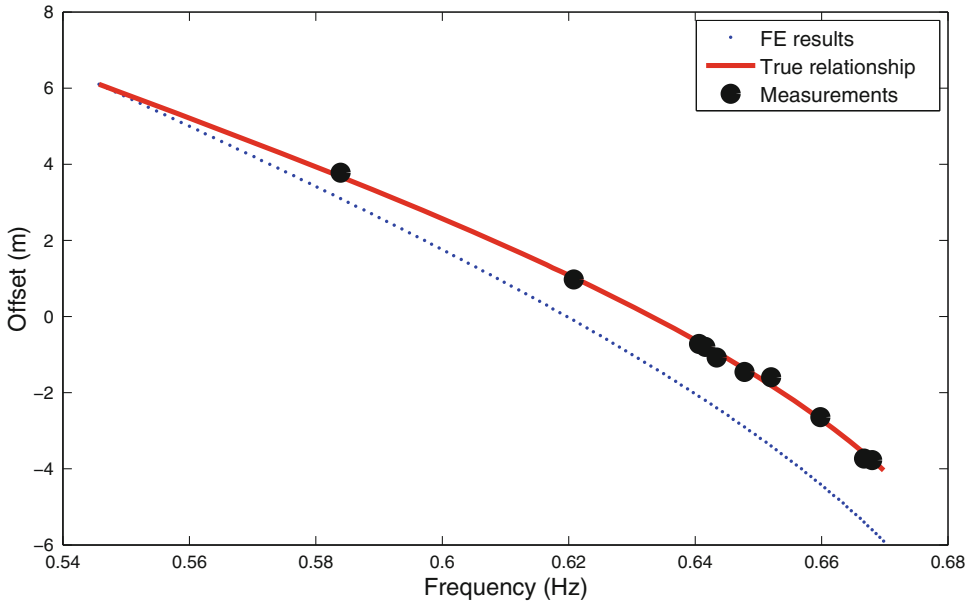

Fig. 2.2 Relation between the first natural frequency of an offshore platform and the vertical offset of its COG. *Blue dots* show results according to the FE model, *black dots* represent available measurement and the *red line* represents the true relationship

where the ijth element of $\boldsymbol{K_2}$ is given by the kernel function

$$k_2(x_i, x_j) = \exp\left(-\frac{\alpha_2}{2}(x_i - x_j)^2\right) \tag{2.5}$$

and α_2 is a second hyperparameter.

2.3.3 Predictions

Say a new frequency measurement, x^*, is obtained. The aim here is to predict the probability of

$$z^* = y(x^*) + \eta(x^*) + \epsilon, \tag{2.6}$$

given the data, $\boldsymbol{d} = (\boldsymbol{y}^T, \boldsymbol{z}^T)^T$. To do so, one can first derive the joint probability density function $p(\boldsymbol{d}, z^*)$ such that, by exploiting some useful properties of Gaussian distributions, it is then be possible to find the conditional distribution $p(z^*|\boldsymbol{d})$. Before proceeding, it is convenient to write $p(\boldsymbol{d})$ in the following form:

$$p(\boldsymbol{d}) = \mathcal{N}(\boldsymbol{0}, \boldsymbol{V_d}), \qquad \boldsymbol{V_d} = \begin{bmatrix} \boldsymbol{V}_1 & \boldsymbol{C} \\ \boldsymbol{C}^T & \boldsymbol{V_2} \end{bmatrix}. \tag{2.7}$$

The ijth element of $\boldsymbol{V_1}$ is given by

$$\mathrm{Cov}[y_i, y_j] = k_1(x_i', x_j') + \beta^{-1}\delta_{ij} \tag{2.8}$$

where β is a hyperparameter whose roll will be explained shortly. The ijth element of $\boldsymbol{C}$ is given by

$$\mathrm{Cov}\left[y_i, z_j\right] = \mathrm{Cov}\left[y(x_i'), y(x_j) + \eta(x_j) + \epsilon_j\right] = \mathrm{Cov}[y(x_i'), y(x_j)] = k_1(x_i', x_j), \tag{2.9}$$

and the ijth element of $\boldsymbol{V_2}$ is given by

$$\begin{aligned} \boldsymbol{V_2} = \mathrm{Cov}[z_i, z_j] &= \mathrm{Cov}[y(x_i) + \eta(x_i) + \epsilon_i, y(x_j) + \eta(x_j) + \epsilon_j] \\ &= \mathrm{Cov}[y(x_i), y(x_j)] + \mathrm{Cov}[\eta(x_i), \eta(x_j)] + \mathrm{Cov}[\epsilon_i, \epsilon_j] \\ &= k_1(x_i, x_j) + k_2(x_i, x_j) + \lambda^{-1}\delta_{ij}. \end{aligned} \tag{2.10}$$

Using a similar approach it can then be shown that

$$p(\boldsymbol{d}, z^*) = \mathcal{N}\left(\boldsymbol{0}, \begin{bmatrix} \boldsymbol{V_d} & \boldsymbol{a} \\ \boldsymbol{a}^T & c \end{bmatrix}\right), \qquad \boldsymbol{a} = \begin{pmatrix} \boldsymbol{a_1} \\ \boldsymbol{a_2} \end{pmatrix} \tag{2.11}$$

where the ith element of $\boldsymbol{a_1}$ is

$$\mathrm{Cov}[y_i, z^*] = k_1(x_i', x^*), \tag{2.12}$$

the ith element of $\boldsymbol{a_2}$ is

$$\mathrm{Cov}[z_i, z^*] = k_1(x_i, x^*) + k_2(x_i, x^*) \tag{2.13}$$

and

$$c = \mathrm{Var}[z^*] = k_1(x^*, x^*) + k_2(x^*, x^*) + \lambda^{-1}. \tag{2.14}$$

Table 2.1 Hyperparameter prior limits

Parameter	Lower limit	Upper limit
α_1	0	1×10^4
α_2	0	1×10^4
β	0	1×10^6

Using the generic properties of Gaussian distributions, the desired conditional distribution is then given by

$$p(z^*|\boldsymbol{d}) = \mathcal{N}(m, \sigma^2) \tag{2.15}$$

where

$$m = \boldsymbol{a}^T \boldsymbol{V_d}^{-1} \boldsymbol{d}, \qquad \sigma^2 = c - \boldsymbol{a}^T \boldsymbol{V_d}^{-1} \boldsymbol{a}. \tag{2.16}$$

2.3.4 *Hyperparameters*

The kernel functions were defined as

$$k_1(x_i, x_j) = \exp\left(-\frac{\alpha_1}{2}(x_i - x_j)^2\right), \qquad k_2(x_i, x_j) = \exp\left(-\frac{\alpha_2}{2}(x_i - x_j)^2\right) \tag{2.17}$$

where α_1 and α_2 are hyperparameters which require estimation. The third hyperparameter, β, is included in Eq. (2.8) simply because, if tuned appropriately, it can be used to avoid numerical errors when calculating the inverse of $\boldsymbol{V_d}$. The vector of hyperparameters which require estimation is therefore $\boldsymbol{\theta} = (\alpha_1 \quad \alpha_2 \quad \beta)^T$.

In the current work the authors endeavored to include hyperparameter uncertainty in the analysis. Bayes' theorem allows the probability of $\boldsymbol{\theta}$ given the data, $\boldsymbol{d}$, to be written as

$$p(\boldsymbol{\theta}|\boldsymbol{d}) \propto p(\boldsymbol{d}|\boldsymbol{\theta}) p(\boldsymbol{\theta}) \tag{2.18}$$

where $p(\boldsymbol{d}|\boldsymbol{\theta})$ is given by Eq. (2.7) and $p(\boldsymbol{\theta})$ was chosen to be a uniform distribution, whose limits are shown in Table 2.1. Samples from the posterior, $p(\boldsymbol{\theta}|\boldsymbol{d})$, were then generated using Markov chain Monte Carlo (MCMC). In this example, the authors used the Transitional MCMC algorithm [5], as it is suitable for parallelisation and can generate samples from distributions with complex geometries. A discussion of various MCMC methods, within the context of structural dynamics, can be found in [6].

2.4 Results

The resulting MCMC samples are shown in Fig. 2.3 while Fig. 2.4 shows the predictions made using the most probable estimates of the hyperparameters. It can be seen that, despite the model error present, the predicted relationship between the first natural frequency and the COG offset closely follows the true relationship.

Monte Carlo simulations were then used to propagate hyperparameter uncertainty into the offset predictions. This can be achieved using 'ancestral sampling', where one first generates a sample from $p(\boldsymbol{\theta}|\boldsymbol{d})$ before going on to generate a sample from $p(z^*|\boldsymbol{\theta}, \boldsymbol{d})$. This is possible in the current case as samples from $p(\boldsymbol{\theta}|\boldsymbol{d})$ have already been obtained using MCMC and $p(z^*|\boldsymbol{\theta}, \boldsymbol{d})$ is given by Eq. (2.15). The mean and variance of one's predictions can then be estimated using the resulting ensemble of predictions. The results of this analysis are shown in Fig. 2.5. It can be seen that, by accounting for this additional source of uncertainty, the confidence bounds have grown in the regions where little measurement data is available.

While these results are promising, one may question whether the additional complexity of this methodology is necessary—could similar results have been achieved if one simply interpolated through the available measurement data, $\boldsymbol{z}$? To that end, a GP with prior

$$p(\boldsymbol{z}) = \mathcal{N}(\boldsymbol{0}, \boldsymbol{K_3}), \tag{2.19}$$

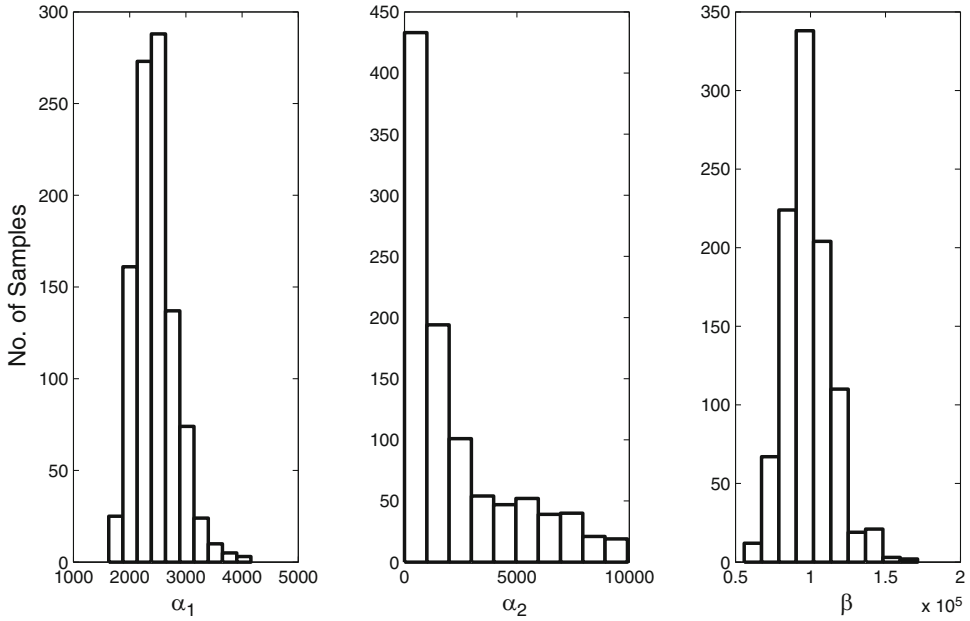

Fig. 2.3 MCMC samples from $p(\boldsymbol{\theta}|\boldsymbol{d})$

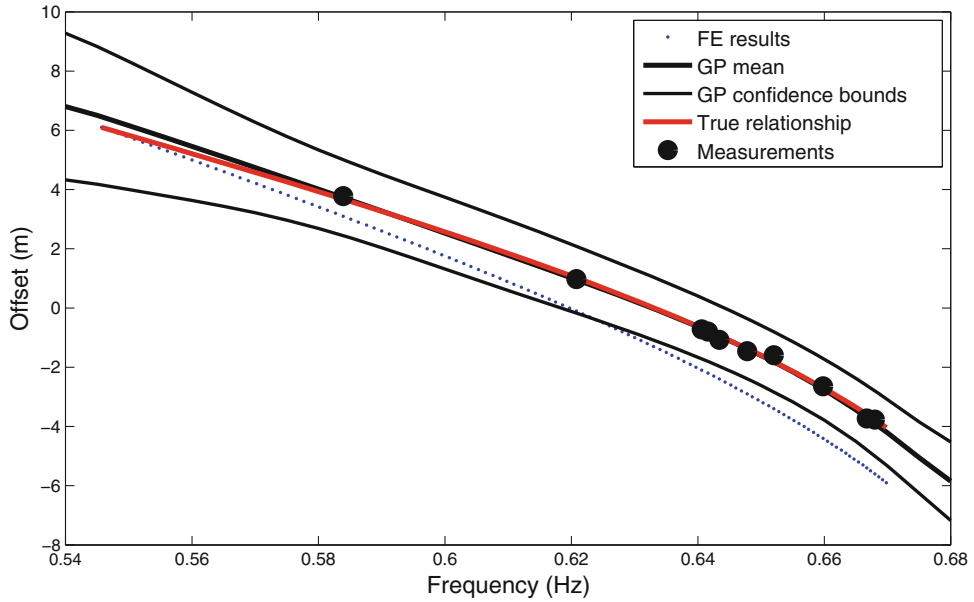

Fig. 2.4 Predictions made using the most probable hyperparameter estimates (with 3 σ confidence bounds)

where the (i,j) element of $\boldsymbol{K_3}$ is given by the kernel function

$$k_3(x_i,x_j) = \exp\left(-\frac{\alpha_3}{2}(x_i-x_j)^2\right) + \lambda^{-1}\delta_{ij}, \tag{2.20}$$

was used to interpolate between $\boldsymbol{z}$. To account for hyperparameter uncertainty, MCMC samples from $p(\alpha_3|\boldsymbol{z})$ were obtained using MCMC (Fig. 2.6). By, again, using Monte Carlo simulations to propagate the hyperparameter uncertainty into the predictions, the results shown in Fig. 2.7 were realised. It is clear that, by using the 'full' framework described in [2], far better predictions have been obtained.

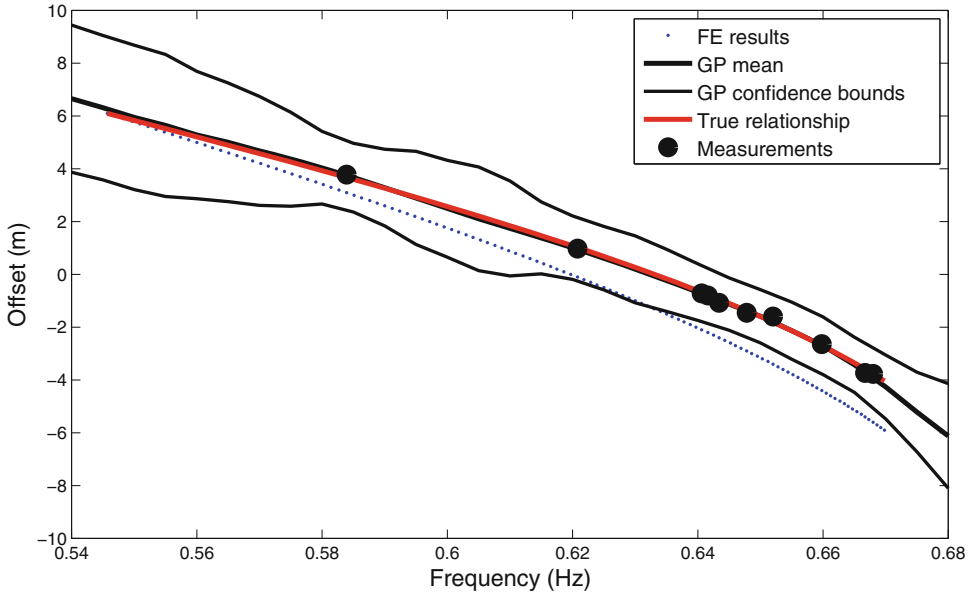

Fig. 2.5 Predictions made accounting for hyperparameter uncertainty (with 3 σ confidence bounds)

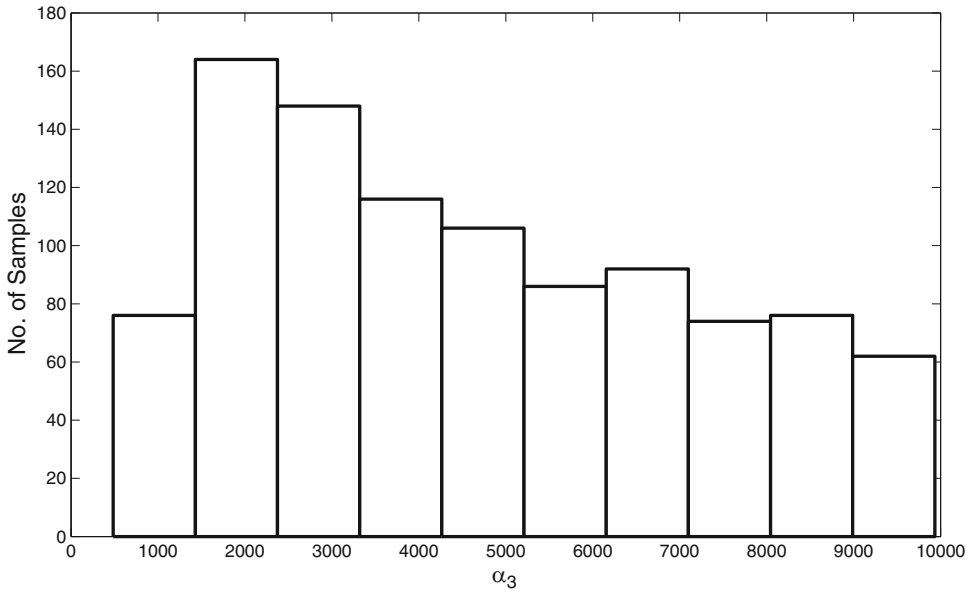

Fig. 2.6 MCMC samples from $p(\alpha_3|z)$

2.5 Conclusions

In this paper, the approach described in [2] was used to aid the model updating of a FE model of an offshore structure. This involved quantifying the uncertainties generated by model error, measurement noise and, through the use of MCMC sampling methods, hyperparameter uncertainty. It emphasises how, by utilising only a sparse set of measurements which are taken during different operational conditions, the accuracy of the updating procedure can be greatly improved.

While the current paper only addressed the updating of a single parameter of the FE model, the authors aim to use this methodology to update the full set of parameters utilised in the bespoke FE models employed by Ramboll Oil & Gas. It is hoped that, by 'compressing' the outputs of the FE model simulations using a Singular Value Decomposition (see [7] for more details), the computational cost of this approach should be kept relatively small.

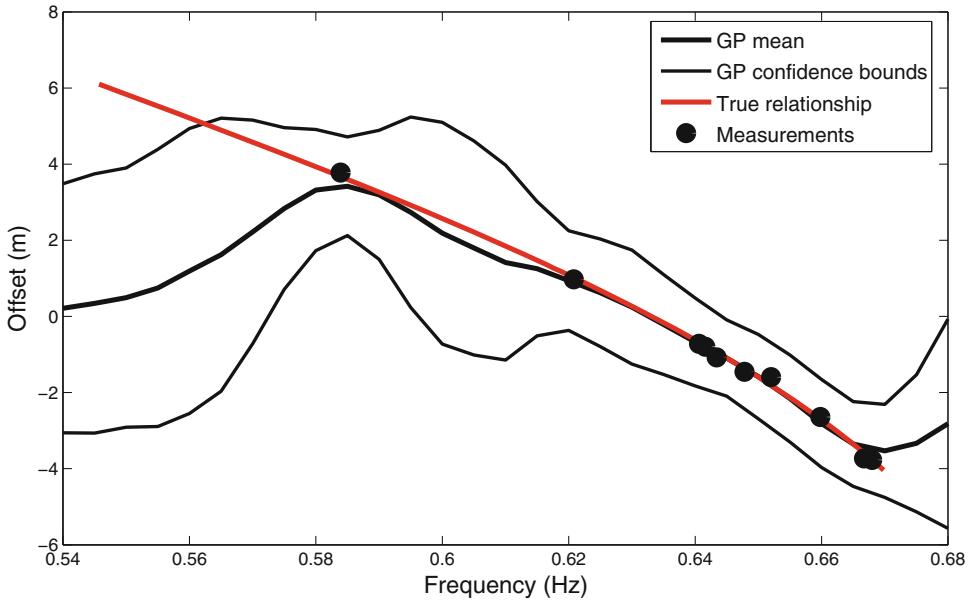

Fig. 2.7 Predictions made by simply interpolating through the available measurement data

References

1. Ramboll Oil & Gas: Ramboll Offshore Structural Analysis Programs (ROSAP). www.ramboll.com/oil-gas.
2. Kennedy, M.C., O'Hagan, A.: Bayesian calibration of computer models. J. R. Stat. Soc. **63**(3), 425–464 (2001)
3. Bishop, C.M.: Pattern Recognition and Machine Learning. Springer, Berlin (2006)
4. MacKay, D.J.C.: Information Theory, Inference and Learning Algorithms. Cambridge University Press, Cambridge (2003)
5. Ching, J., Chen, Y.C.: Transitional Markov chain Monte Carlo method for Bayesian model updating, model class selection, and model averaging. J. Eng. Mech. **133**(7), 816–832 (2007)
6. Green, P.L., Worden, K.: Bayesian and Markov chain Monte Carlo methods for identifying nonlinear systems in the presence of uncertainty. Philos. Trans. R. Soc. A **373**(2051), 20140405 (2015)
7. Higdon, D., Gattiker, J., Williams, B., Rightley, M.: Computer model calibration using high-dimensional output. J. Am. Stat. Assoc. **103**(482), 570–583 (2008)

http://www.springer.com/978-3-319-29753-8

Model Validation and Uncertainty Quantification, Volume 3
Proceedings of the 34th IMAC, A Conference and Exposition on Structural Dynamics 2016
Atamturktur, S.; Schoenherr, T.; Moaveni, B.; Papadimitriou, C. (Eds.)
2016, VIII, 379 p. 258 illus., 215 illus. in color., Hardcover
ISBN: 978-3-319-29753-8